^{1}H NMR study of residual HNO_3-intercalated graphite

E. M. Kunoff, S. D. Goren, and C. Korn
Department of Physics, Ben-Gurion University of the Negev, P.O. Box 653, 84 105 Be'er-Sheva, Israel

H. Riesemeier, I. Stang, and K. Lüders
Institut für Atom- und Festkörperphysik, Freie Universität Berlin, D-1000 Berlin 33, West Germany
(Received 22 September 1988)

The proton spin-lattice relaxation time T_1 of residual stage-3 HNO_3-intercalated graphite has been measured as a function of temperature over the range 8–310 K. We observe two relaxation times over the temperature range 8–180 K and four relaxation times in the range 180–310 K. We observe changes in slope at 40, 90, 180, 210, and 250 K. The Fourier transform of the free induction decay consists of three lines: a central peak with two satellites. The angular dependence of the satellites is fitted with a Lorentzian convolution of the spectrum of a conically averaged Pake doublet. This analysis assumes that in one structural phase, pairs of HNO_3 molecules hydrogen bond to form a dimer. Interatomic distances in such a molecule conform to a commensurate $(\sqrt{7}\times\sqrt{7})R\,19.11°$ orientation with respect to the graphite lattice. The existence of several T_1 values requires the existence of a second structural phase in islands separate from the first; this is proposed as $(\sqrt{3}\times\sqrt{3})R\,0°$ based on the sample stoichiometry.

I. INTRODUCTION

Interest in graphite intercalation compounds as a testing ground for two-dimensional phenomena has led to many recent studies of molecular diffusion and structural phase transitions in nitric acid–intercalated graphite.[1–5] This particular graphite intercalation compound (GIC) exists in two forms. When the ordinary form, α-$C_{5n}HNO_3$, is exposed to air or N_2 gas for an extended time period, the HNO_3 molecules, which stand essentially perpendicular to the graphite planes, reorient to lie nearly parallel, yielding the more dilute β-$C_{8n}HNO_3$ residue compound. Here n denotes the stage, the number of graphite planes between intercalate layers, of the GIC. Because synthesis of the residue compound is difficult and time consuming, most studies of HNO_3-GIC's have been confined to the α type; we have therefore concentrated the present NMR studies to temperature-induced structural phase transitions in the residue compound.

^{1}H NMR,[1,2,6] ^{13}C NMR,[5] x-ray,[3,6–9] and quasielastic neutron scattering[4,10] spectroscopies have detected structural phase transitions in α-type HNO_2-GIC's at approximately 210 and 250 K. The latter transition has been observed in calorimetry[11] and conductivity[12,13] measurements as well. Differential thermal analysis reveals an additional phase transition at 133 K, attributed to the freezing out of rotational motions of the nitric anions.[14] In the low-temperature phases, the HNO_3 molecules form a lattice commensurate with the graphite, while between 210 and 250 K they form a striped domain phase, commensurate with the graphite lattice along one $\hat{\mathbf{a}}$ direction and discommensurate along the perpendicular in-plane direction.[9] Above 250 K the HNO_3 molecules have no long-range order and constitute a lattice liquid. Similar behavior has been observed in other molecular-acceptor GIC's, most notably Br_2 (Ref. 15) and $SbCl_5$.[16]

In this paper we report the results of proton NMR of a stage-3 β-type HNO_3-GIC over the temperature range 8–310 K. Section II contains the experimental details and our results are analyzed in Sec. III with the exception of the angular dependence whose analysis is relegated to the appendix. We propose a crystalline structure for the intercalate which can explain our results.

II. EXPERIMENTAL DETAILS

All measurements were made on several stacked slabs of HNO_3-GIC's characterized by (00l) x-ray diffraction as stage 3 with graphite-intercalate layer thickness $d_i = 6.55$ Å corresponding to that of the residue compound. Weight uptake measurements yield a formula for this sample of $C_{19}HNO_3$ which contains more intercalate than the $C_{8n}HNO_3$ reported in the literature.[17] No more than $\sim 5\%$ of the sample consists of α-$C_{15}HNO_3$. The sample size is $15\times10\times10$ mm^3. Details of the sample preparation are given in Ref. 18.

Proton Fourier-transform (FT) NMR measurements were made at a resonance frequency of 47 MHz over the temperature range of 8–310 K. The results were obtained using a single excitation pulse of 1 μsec and recording the free induction decay (FID) after the pulse. The absorption signal for various temperatures is given in Fig. 1. We observe a central peak and a symmetric doublet which we assign to separate intercalate structures. The spin lattice relaxation time T_1 was obtained by Fourier transforming the FID signal after a saturation sequence and measuring the rate of growth of area of a window of ~ 2.5 kHz centered at the central peak and at one of the satellites. When the sample is oriented with $\mathbf{H}_0 \| \hat{\mathbf{c}}$, the recovery of the area under the doublet can only be

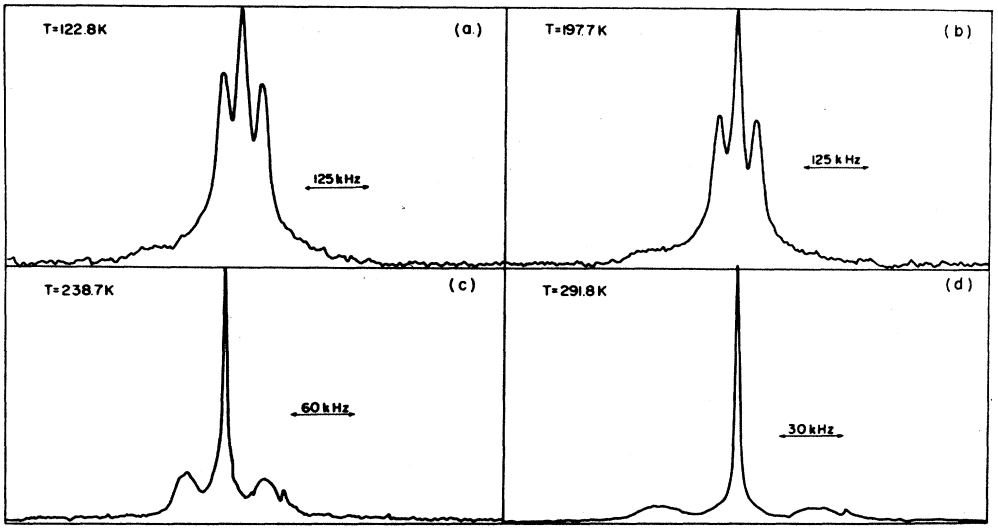

FIG. 1. ^{1}H absorption spectra of nitric acid intercalated graphite taken with $\mathbf{H}_0 \perp \hat{c}$ at temperatures (a) 291.8 K, (b) 238.7 K, (c) 197.7 K, and (d) 122.8 K. Graphs are normalized to the maximum value of the central peak.

fitted using two relaxation times whereas one is sufficient for the perpendicular orientation. Above ~ 190 K we could not saturate the central line and only the T_1 of the satellites was obtained by this procedure. In order to measure the T_1 of the central line, we used the inversion recovery method at 18, 47, and 60 MHz. In all cases, the rate of growth of the magnetization could not be fit with one exponential, indicating a return to equilibrium with more than one relaxation rate.

III. EXPERIMENTAL RESULTS AND DISCUSSION

We measured both the temperature and the orientational dependence of the NMR parameters. While we

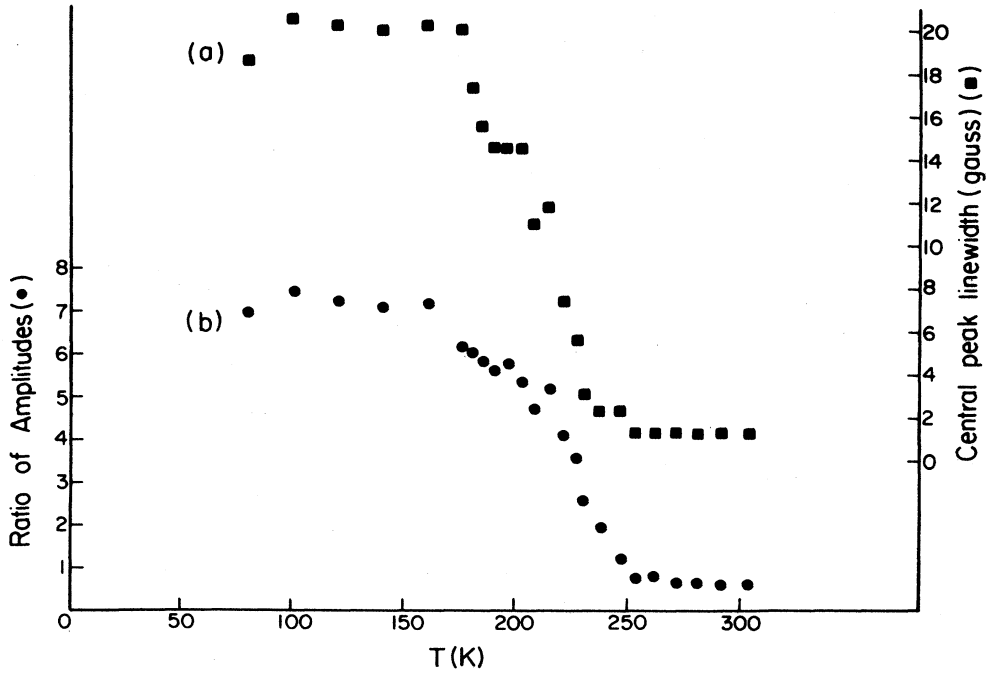

FIG. 2. (a) FWHM of the central peak and (b) ratio of the amplitude of the central peak to the amplitude of the satellites in the absorption spectra with $\mathbf{H}_0 \perp \hat{c}$ as a function of temperature over the range 30–310 K.

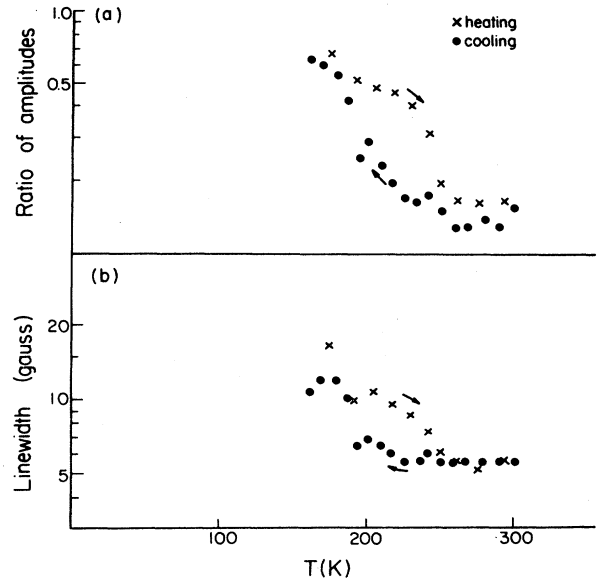

FIG. 3. Hysteresis of the (a) ratio of the central peak amplitude to satellite amplitude and (b) FWHM of the central peak over the temperature range 180–250 K for $\mathbf{H}_0 \| \hat{c}$.

found no orientational dependence of T_1, there was such a dependence of the shape of the satellite doublet. We first present the temperature dependence of the NMR parameters. Figure 1 shows four absorption spectra taken with $\mathbf{H}_0 \perp \hat{c}$ at the temperatures 122.8, 197.7, 238.7, and 291.8 K. In the succeeding discussion it will be shown that these traces are representative of four different phases. This is seen in the significant differences in the intensities of the satellite peaks relative to that of the central peak and in the linewidth of the central peak itself at the four temperatures. The temperature dependence of these parameters is presented in Fig. 2: (a) the central peak linewidth and (b) the ratios of the satellite to central peak amplitudes. We have also studied the effect of cycling the temperature on the line shapes and find a hysteresis around 180–250 K. The amplitude ratios and the central peak width for these traces are plotted as a function of temperature in Figs. 3(a) and 3(b), respectively. Using a waiting time of several hours at one temperature had no effect on the data, in contrast to what de Groot *et al.*[19] found for $SbCl_5$-intercalated graphite.

The results of our T_1 measurements as a function of temperature are seen in Figs. 4 and 5. The most striking feature of our T_1 data is the coexistence of several distinct T_1 values at all temperatures. Within our experimental error, we found no orientational dependence of T_1, as opposed to the line shape of the doublet in the FT: the doublet is found to have less overlap with the central line for $\mathbf{H}_0 \perp \hat{c}$ than when $\mathbf{H}_0 \| \hat{c}$. Hence, we were generally able to fit the data to a single relaxation time separately for the doublet and the central line when $\mathbf{H}_0 \perp \hat{c}$. We label these T_1^d and T_1^c (doublet, central), respectively. When $\mathbf{H}_0 \| \hat{c}$, there is significant overlap of the peaks and the recovery of the area under the window of the doublet can only be fit using two relaxation times. It is found that the two values of T_1 coincide with the curves of T_1^d and T_1^c. In Fig. 4, these are plotted on a log scale as a function of temperature over the entire temperature range studied by the saturation recovery method. The relaxation times of the doublet are quite long, ranging from tens of seconds to nearly half an hour at the lowest temperatures

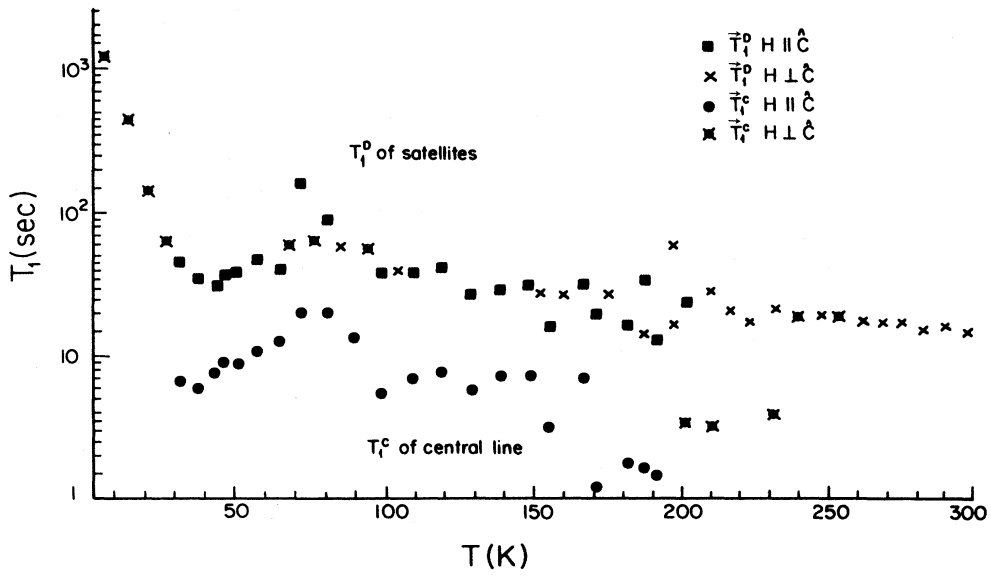

FIG. 4. Log of T_1 as function of temperature over the range 8–300 K for $\mathbf{H}_0 \| \hat{c}$ and $\mathbf{H}_0 \perp \hat{c}$ measured at resonant frequency 47 MHz. The upper (lower) curve is T_1^d (T_1^c) of text.

reached, while the corresponding T_1^c of the central peak is consistently an order of magnitude smaller. At approximately 190 K we were no longer able to saturate the central peak with a comb of pulses due to the onset of a much shorter T_1 probably resulting from the presence of a new structural phase. This phase apparently does not occur in the structure giving rise to the satellite peaks as we were able to continue saturation recovery measurements on them up to 310 K; the data points above 190 K in Fig. 4 were obtained from the saturation recovery of the satellite peaks alone. We note that at this same temperature the amplitude of the satellites begins to decrease relative to the central peak.

In the high temperature region, we measured the much shorter T_1 which appears using the inversion recovery method. Because the long T_1 in this region is of the order of tens of seconds, a pulse repetition rate that would permit its measurement is prohibitively long, so we used a faster rate which saturated that portion of the signal and could measure only the newly appearing shorter relaxation times, again obtaining two distinct T_1 values. These are labeled $T_{1,l}^c$ and $T_{1,s}^c$ in the plot of $\log T_1$ as a function of $1/T$ for the high-temperature region in Figs. 5(a) and 5(b), respectively. We note a break in $T_{1,l}^c$ at 210 K and a break in $T_{1,s}^c$ at 250 K, similar to the results of Avogadro and Villa[2] for ordinary HNO_3 GIC's. Another important feature is that the minimum in T_1 at about 200 K has essentially the same value for all three resonant frequencies, evidence that it is due to a phase transition and not to the motionally induced minimum predicted by Bloemberger-Purcell-Pound theory.[20] We find this behavior to be orientationally independent.

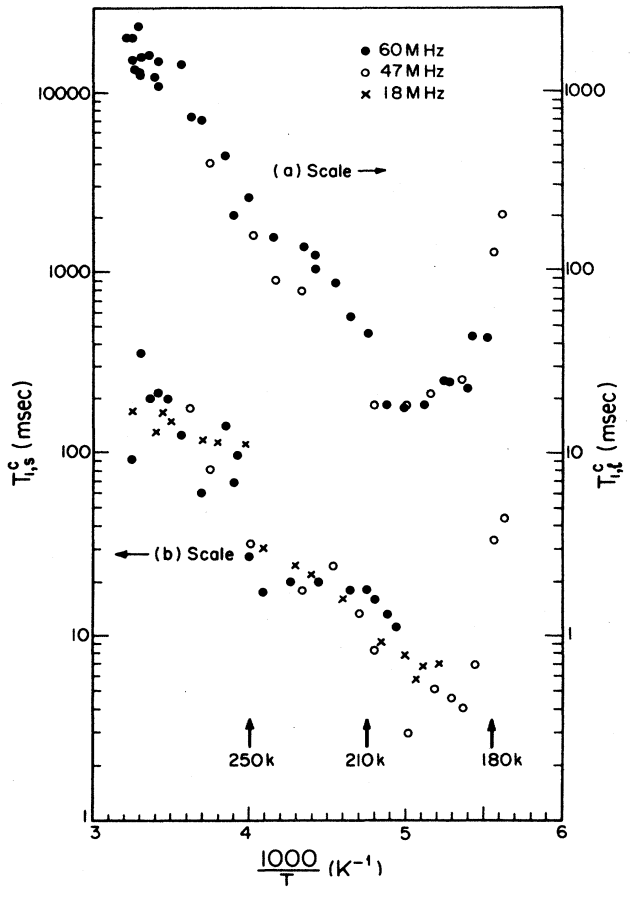

FIG. 5. Log scale plots of (a) $T_{1,l}^c$ and (b) $T_{1,s}^c$ vs 1000/T with $\mathbf{H}_0 \perp \hat{c}$. Temperatures of phase transitions are marked with arrows.

Figures 1–5, when considered together, provide strong evidence for several structural phase transitions occurring in this intercalation compound. Beginning with the highest-temperature transition, we note discontinuities in the traces of Figs. 2(a), 2(b), and 5(b) at 250 K and the end of the hysteresis in Figs. 3(a) and 3(b) at this same temperature. Figure 5(a) exhibits a sharp break at 210 K which is accompanied by a large change of slope in the relative amplitudes plotted in Fig. 2(b). Weaker features at this temperature are noted in Figs. 2(a) and 4. The other end of the hysteresis loops in Figs. 3(a) and 3(b) occurs at 180 K as do discontinuities in the linewidths, relative amplitudes and short T_1 values, most notably in Figs. 2 and 5(b). All these data support a model of four different structural phases, each represented by one of the four absorption spectra in Fig. 1. Extrema in the T_1 data are noted at 42 and 75 K, indicating the possible presence of additional lower temperature phases. The discontinuities at 210 and 250 K were also found for α-HNO_3-GIC's where the 210-K transition was attributed to a change from a commensurate to a semi-incommensurate phase[3] accompanied by rotational HNO_3 motion[21] and the 250-K transition is to a lattice liquid state[3] accompanied by translational motion.[21]

In Fig. 6 we show the free induction decay from which the Fourier transform was taken close to the transition near 180 K. In the trace at 182.3 K we note the presence of only quickly decaying oscillations. At $T=187.4$ K, we begin to see an additional oscillation with very small amplitude and much longer decay time, T_2. The amplitude of the latter increases with the temperature and by $T=191.3$ K is a prominent feature of the decay, while the short decay remains practically unchanged. This is a vivid demonstration of the emergence of the new phase having a long T_2 and short T_1 [as seen in Fig. 5(a)] as the temperature is increased above 180 K.

Another important feature of the Fourier-transform spectra is the dependence of the line shape on the angle between the $\hat{c}$ axis and $\mathbf{H}_0$, seen in Fig. 7, spectra taken at $T=235$ K. At small angles θ, from about 0° to 30°, the satellites each split to two distinct peaks which eventually merge at the position of the inner frequency peak, become narrow at approximately 60°, then broaden and move out from the center around 90°. This behavior is explained on the basis of a particular ordered in-plane structure wherein two HNO_3 molecules are hydrogen bonded resulting in a pairing of hydrogen atoms giving a Pake doublet.

The existence of the satellites and the dependence of their shape on the angle between the $\hat{c}$ axis and the magnetic field leads us to conclude that there exists a struc-

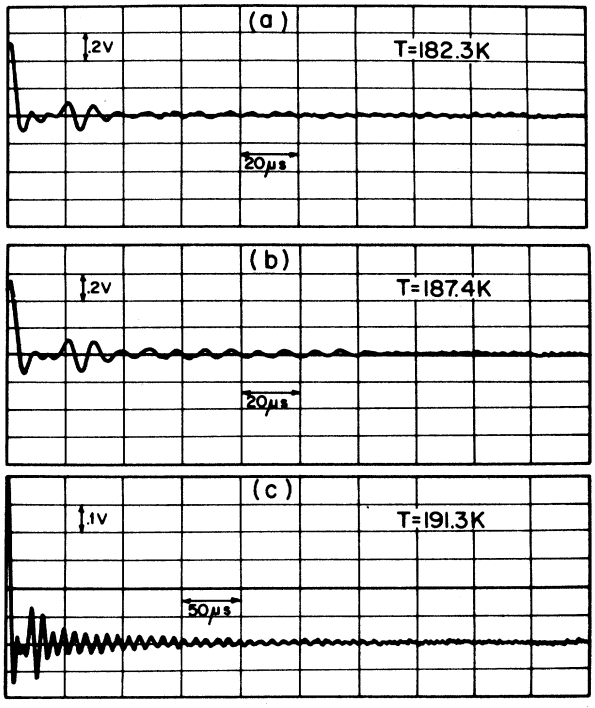

FIG. 6. Free induction decay at resonant frequency 47 MHz with $\mathbf{H}_0$ at 45° to $\hat{c}$ for temperatures (a) 182.3 K, (b) 187.4 K, and (c) 191.3 K. Similar results were obtained at other orientations. Note the change of time scale in (c).

ture in which the hydrogen atoms form pairs with fixed distances between them and the line connecting them makes a fixed angle β with the $\hat{c}$ axis. The details of how this model yields the observed behavior is given in the Appendix. The second coexisting structure consists of unpaired HNO_3 molecules, giving rise to the central line. A possible structure wherein the hydrogen lie close enough for the pairing giving rise to the doublet could be a commensurate phase of $C_{7n}HNO_3$. The unit cell relative to the graphite host, $(\sqrt{7}\times\sqrt{7})R19.11°$ is illustrated in Fig. 9(b).

As noted in Sec. II, the chemical formula of our stage-3 sample is $C_{19}HNO_3$, lying between $C_{6n}HNO_3$ and $C_{7n}HNO_3$. A commensurate phase must therefore consist of domains of each structure separated by boundary walls of HNO_3 molecules in slightly incommensurate positions. The commensurate orientations of (a) $C_{6n}HNO_3$ and (b) $C_{7n}HNO_3$ are depicted in Fig. 8. The unit cell relative to that of the graphite host corresponding to $C_{6n}HNO_3$ is $(\sqrt{3}\times\sqrt{3})R0°$. We note that the $C_{7n}HNO_3$ unit cell contains two HNO_3 molecules which are sufficiently close to allow hydrogen bonding of an oxygen atom from each molecule as indicated by the dotted lines in the figure, thus forming a Pake doublet. Specifically, this model predicts an intermolecular O-O distance of $\sim$2.33 Å and an intramolecular O-O distance of 1.96 Å where in each case a H atom is associated with one of the oxygens. We assume that one lies above and the other below the NO_3 plane, separated by the inter-proton vector $r=1.5$ Å as calculated from the theory for a conically averaged Pake doublet discussed below. Although the nitric acid is more dilute in the $C_{7n}HNO_3$ compound, the HNO_3 molecules are more evenly spaced in the $C_{6n}HNO_3$ commensurate orientation so that the shortest intermolecular O-O distance of 4.25 Å is considerably longer than in $C_{7n}HNO_3$. Again, the average inter-proton separation depends on the exact position of each H atom with respect to the O to which it is bonded, but is clearly longer than in the $C_{7n}HNO_3$ orientation.

Above approximately 180 K, the thermal energy is sufficient to break the hydrogen bonds. Hence at this temperature one can expect the HNO_3 dimers to begin to

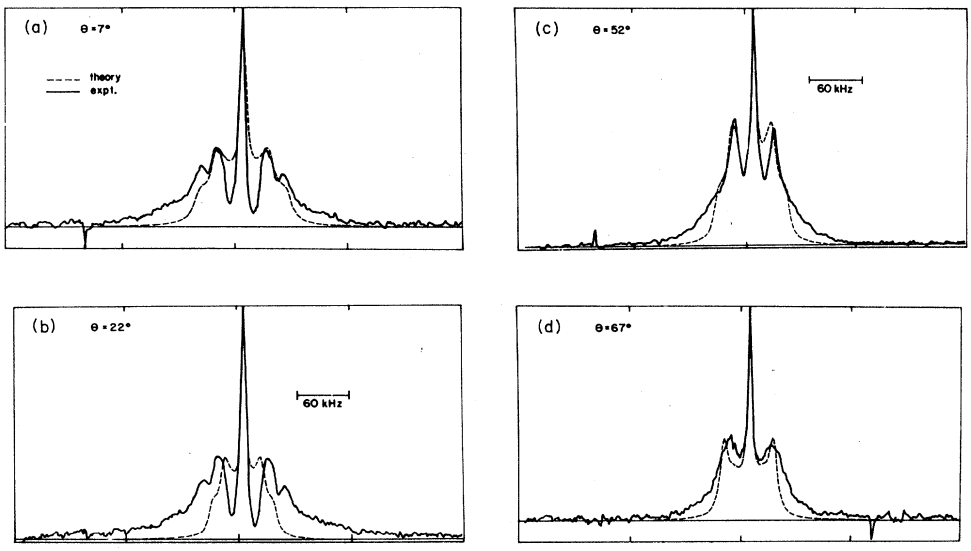

FIG. 7. Fit of conically averaged Pake doublet theoretical line shape (dotted line) to experimental data (solid line) for angles (a) 7°, (b) 22°, (c) 52°, and (d) 67° between $\mathbf{H}_0$ and $\hat{c}$ for $\beta=25°$, $\nu_D=25$ kHz, and $\sigma=5$ kHz. Data were taken at $T=235$ K.

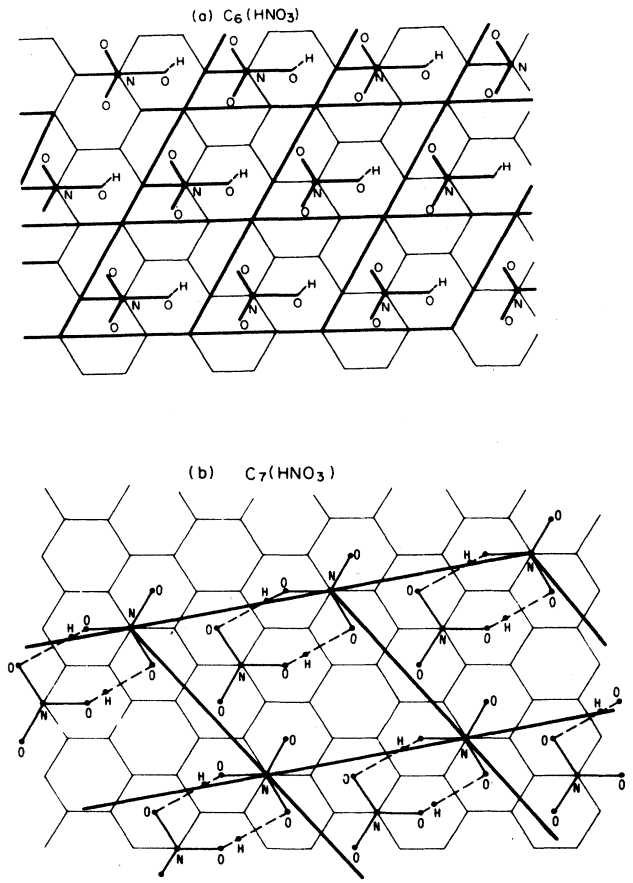

FIG. 8. In-plane ordering of HNO_3 molecules in (a) C_{6n} HNO_3 and (b) $C_{7n}HNO_3$. Vertices of honeycomb represent C atoms of the graphite plane, large solid circles are O atoms, smaller solid circles are N atoms, and the smallest solid circles are H atoms which are placed only schematically and lie above and below the N-O plane. Dashed lines represent hydrogen bonds between O atoms which are not linear.

break up, yielding the observed increase in the central line intensity with respect to the satellites. Additionally, the HNO_3 molecules of both structures would rotate, resulting in the observed central peak line narrowing and the emergence of the wiggles previously discussed in context with Fig. 6. The two T_1's of the central line can also be attributed to these separate structures ($C_{6n}HNO_3$ and the broken dimers in $C_{7n}HNO_3$).

The angular dependence of the satellite peaks is well described by a conical average of a Pake doublet convoluted by a Lorentzian line,[22] as seen by the fits of this theory to our data for $\theta=7°$, 22°, 52°, and 67° in Fig. 7. Since highly oriented pyrolitic graphite (HOPG), the host lattice of our sample, consists of small crystallites with randomly oriented $\hat{\mathbf{a}}$ axes and well aligned $\hat{\mathbf{c}}$ axes, with a mosaic spread of less than 2°, one takes a conical average. To account for the Pake doublet, we must assume a structure in which hydrogen atoms from two different HNO_3 molecules are sufficiently close to form a pair. This condition is met for the commensurate unit cell of the $C_{7n}HNO_3$ structure, as seen in Fig. 8(b). The greater spread in our experimental data is attributed to the presence of several stacked samples, causing more misalignment of the $\hat{\mathbf{c}}$ axis, estimated at $\sim 10°$. Additional spread is due to the contribution of H atoms in the domain walls at discommensurate positions.

Two parameters of our fits to the data are the angle β between the proton-proton vector and the graphite $\hat{\mathbf{c}}$ axis and ν_D, the dipolar splitting,

$$\nu_D=\frac{3\gamma\hbar}{4r^3}\ , \tag{1}$$

where γ is the proton gyromagnetic ratio and r the interproton distance. We obtain a value of $28°\pm4°$ for β, indicating that the H atoms are well out of the NO_3 plane. Using our derived value for ν_D in Eq. (1), we obtain $r=1.5\pm0.1$ Å, consistent with our proposed unit cell. More specifics of the theory of a Pake doublet in a two-dimensional powder are presented in the Appendix.

ACKNOWLEDGMENTS

We would like to thank Professor R. Moreh for providing us with the sample and for useful discussions. This research was supported by the Fund for Basic Research administered by the Israel Academy of Sciences and Humanities (Jerusalem, Israel). One of us (E.M.K.) was partially supported by the Israeli Ministry of Absorption.

APPENDIX: CONICAL AVERAGE OF A PAKE DOUBLET

In this Appendix, we derive the conical average of the dipole-dipole interaction of a pair of two spin-$\frac{1}{2}$ nuclei separated by a distance r. This interaction splits the central line into a doublet, known as the Pake doublet.[23] The resulting expression was fit to our Fourier transform data taken at 235.1 K for different orientations of the sample $\hat{\mathbf{c}}$-axis with respect to the magnetic field $\mathbf{H}_0$. The graphite $\hat{\mathbf{c}}$ will be the $\hat{\mathbf{z}}$ axis. We can express the vectors $\hat{\mathbf{r}}$ and $\hat{\mathbf{H}}_0$ in terms of their angular components,

$$\begin{aligned}\mathbf{r}&=r(\sin\beta\cos\phi\hat{\mathbf{x}}+\sin\beta\sin\phi\hat{\mathbf{y}}+\cos\beta\hat{\mathbf{z}})\ ,\\ \mathbf{H}_0&=H_0(\sin\theta\hat{\mathbf{x}}+\cos\theta\hat{\mathbf{z}})\ ,\end{aligned} \tag{A1}$$

where θ is the angle between $\mathbf{H}_0$ and the graphite $\hat{\mathbf{c}}$ axis and β is the angle between the interproton vector and this axis in the azimuthal angle ϕ has a random distribution around the $\hat{\mathbf{c}}$ axis in the xy plane. Using the dot product, the angle α between $\hat{\mathbf{r}}$ and $\mathbf{H}_0$ is given by

$$\cos\alpha=\sin\theta\sin\beta\cos\phi+\cos\theta\cos\beta\ . \tag{A2}$$

The shift of the frequency of one of the doublets is given by

$$\nu=\nu_D(3\cos^2\alpha-1)=\nu_D[(a\cos\phi+b)^2-1]\ , \tag{A3}$$

if we define

$$F_1(\nu)=\left\{\left[1+\frac{\nu}{\nu_D}\right]\left[a+b+\left[1+\frac{\nu}{\nu_D}\right]^{1/2}\right]\times\left[a-b-\left[1+\frac{\nu}{\nu_D}\right]^{1/2}\right]\right\}^{-1/2}\ , \tag{A4}$$

where $a=\sqrt{3}\sin\theta\sin\beta$ and $b=\sqrt{3}\cos\theta\cos\beta$. Then for

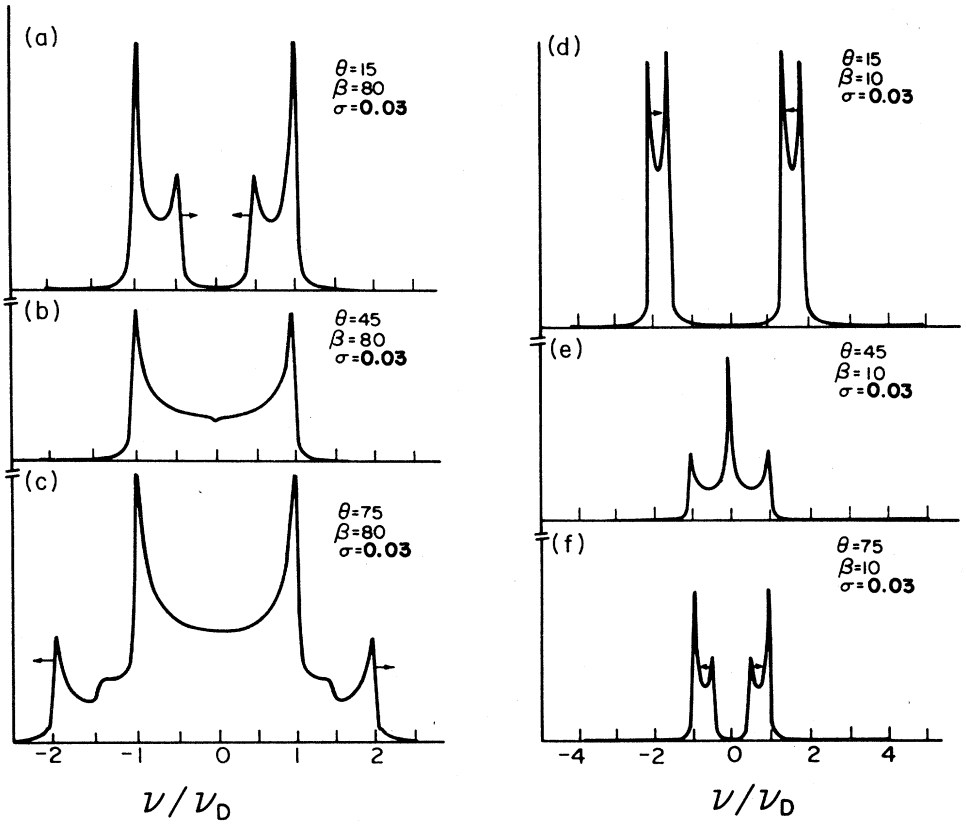

FIG. 9. Calculated curve of conically averaged Pake doublet convoluted with a Lorentzian with width $\nu_D=1$ and $\sigma=0.03$ for $\beta=10°$, (a) $\theta=15°$, (b) $\theta=45°$, and (c) $\theta=75°$ and for $\beta=80°$, (d) $\theta=15°$, (e) $\theta=45°$, and (f) $\theta=75°$ (see Appendix).

$a>0$, $b>0$, and $a\geq b$ (case I), the probability density $F(\nu)$ of one member of the doublet is given by

$$F(\nu)=\begin{cases}2F_1(\nu) \text{ for } -1\leq\nu/\nu_D<(a-b)^2-1\ , & \text{(A5a)}\\ F_1(\nu) \text{ for } (a-b)^2-1\leq\nu/\nu_D<(a+b)^2-1, & \text{(A5b)}\\ 0 \text{ otherwise}\ . & \text{(A5c)}\end{cases}$$

If $a>0$, $b>0$ but $a<b$ (case II),

$$F(\nu)=\begin{cases}F_1(\nu) \text{ for } (a-b)^2-1\leq\nu/\nu_D<(a+b)^2-1 & \text{(A6a)}\\ 0 \text{ otherwise}\ . & \text{(A6b)}\end{cases}$$

The restriction $a>0$ and $b>0$ limits our discussion to $0\leq\theta\leq\pi/2$ and $0\leq\beta\leq\pi/2$. The extension to other angles is easily obtained.

When the above expression is convoluted with a Lorentzian line shape we obtain

$$P(\nu)=2\int_{-1}^{(a-b)^2-1}F_1(\nu')\frac{1}{1+\left[\frac{\nu-\nu'}{\sigma}\right]^2}d\nu' + \int_{(a-b)^2-1}^{(a+b)^2-1}F_1(\nu')\frac{1}{1+\left[\frac{\nu-\nu'}{\sigma}\right]^2}d\nu' \quad \text{(A7)}$$

(case I) and

$$P(\nu)=2\int_{(a-b)^2-1}^{(a+b)^2-1}F_1(\nu')\frac{1}{1+\left[\frac{\nu-\nu'}{\sigma}\right]^2}d\nu' \quad \text{(A8)}$$

(case II). The expression can be integrated by parts to remove the singularities. To obtain the full spectrum, one must take the sum $P(\nu)+P(-\nu)$. A sample of the calculations for $\nu_D=1$, $\beta=10°$ and 80° and $\theta=15°$, 45°, and 75° is given in Fig. 9 for $\sigma=0.03\nu_D$.

[1]A. Avogadro and M. Villa, J. Chem. Phys. **70**, 109 (1979).
[2]A. Avogadro and M. Villa, J. Chem. Phys. **66**, 2359 (1977).
[3]E. J. Samuelsen, R. Moret, H. Fuzellier, M. Klatt, M. Lelaurain, and H. Hérold Phys. Rev. B **32**, 417 (1985).
[4]H. Zabel (unpublished).
[5]J. Conard, *Intercalation Compounds of Graphite V* (Acedamon, Jerusalem, Israel, 1987).
[6]H. Fuzellier, Thèse d'Etat, Université de Nancy I, France, 1974

(unpublished).
[7]D. E. Nixon, G. S. Parry and A. R. Ubbelohde, Proc. R. Soc. London, Ser. A **291**, 324 (1966).
[8]G. S. Parry, Mater. Sci. Eng. **31**, 99 (1977).
[9]R. Moret, R. Comès, G. Furdin, H. Fuzellier, and F. Rousseaux, Mater. Res. Soc. Symp. Proc. **20**, 27 (1983).
[10]H. Shaked, H. Pinto, and M. Melamud, Phys. Rev. B **35**, 838 (1986).
[11]A. Dworkin and A. R. Ubbelohde, Carbon **16**, 291 (1978).
[12]A. R. Ubbelohde, Proc. R. Soc. London, Ser. A **304**, 25 (1968).
[13]F. L. Vogel, Carbon **14**, 175 (1976).
[14]A. Avogadro, G. Bellodi, A. Borghesi, G. Samoggia, and M. Villa, Il Nuovo Cimento **38B**, 403 (1977).
[15]A. Erbil, A. R. Kortan, R. J. Birgeneau, and M. S. Dresselhaus, Phys. Rev. B **28**, 6329 (1983).
[16]H. Homma and R. Clarke, Phys. Rev. Lett. **52**, 629 (1984).
[17]H. Fuzellier, J. Melin, and A. Hérold, Mater. Sci. Eng. **31**, 91 (1977).
[18]R. Moreh, O. Shahal, and G. Kimmel, Phys. Rev. B **33**, 5717 (1986).
[19]K. de Groot, V. Müller, D. Maurer, V. Geiser, and H.-J. Güntherodt, in Proceedings of the Carbon Conference, Baden-Baden, 1986 (German Ceramics Society), p. 508 (unpublished).
[20]A. Abragam, *The Principles of Nuclear Magnetism* (Clarendon, Oxford, 1961).
[21]F. Batallan, I. Rosenman, A. Magerl, and H. Fuzellier, Phys. Rev. **32**, 4810 (1985).
[22]Z. Luz, R. Poupko, and E. T. Samulski, J. Chem. Phys. **74**, 5825 (1981).
[23]See, for instance, B. C. Gerstein and C. R. Dybowski, *Transient Techniques in NMR of Solids* (Academic, New York, 1985), p. 97.